Design and characteristics of a non-contact rotational sensor based on a fiber Bragg grating*

LU Li-dan (鹿利单)[1], **LI Hong** (李红)[1], **YAO Qi-feng** (姚齐峰)[1], **HE Wei** (何巍)[1], **and ZHU Lian-qing** (祝连庆)[1,2]**

1. *Beijing Key Laboratory for Optoelectronics Measurement Technology, Beijing Engineering Research Center of Optoelectronic Information and Instruments, Beijing Information Science and Technology University, Beijing 100016, China*
2. *Beijing Laboratory for Biomedical Detection Technology and Instrument, Beijing Information Science and Technology University, Beijing 100192, China*

(Received 27 July 2016)

We propose a novel non-contact rotational sensor based on a fiber Bragg grating (FBG) packaged in a core of a magnetic head, which converts the introduced strain from the circular magnetic railings ruler into the rotational information. A mathematical model is built for processing the data obtained by an interrogator, and the accuracy and resolution of the measurements are analyzed by altering the radius and period of the circular magnetic railings ruler, as well as the dimension of the sensor. The experimental results show that it is in good accordance with the theoretical analysis on rotational angle, and the fitting results indicate that the results obtained from the rotational sensor match very well with the real rotational velocity with a linearity of 0.998 and a standard error of about 0.01.

Document code: A **Article ID:** 1673-1905(2016)06-0421-5

DOI 10.1007/s11801-016-6172-5

Due to its intrinsic merits, such as small size, light weight, anti-electromagnetic interference and easy multiplexing, the fiber Bragg grating (FBG) is currently one of the most promising passive sensors[1-4]. Additionally, fiber optic sensors can be easily connected in series and in parallel to form the quasi-distributed and multiplex arrays, respectively. The wavelength of the fiber grating reflection spectrum would drift back and forth as a silica-based fiber suffers from the variation of the physical factors, such as the temperature, strain and refractive index. We have made a variety of FBG sensors with this technique[5-7].

Angular displacement, rotational velocity and rotational acceleration sensors have been widely used in the automatic control of precision instrument, defense and military fields, and chemical and biological applications[8]. However, it is difficult to directly use optical fiber sensors to measure angular displacement or rotational velocity due to their fragility and limited measuring range[9]. So far, a number of optical fiber displacement sensors have been reported. Angular displacement sensors based on a Fabry-Perot cavity fiber[10] possess a high precision, but they are expensive. Wang Jun et al[11] designed a non-contact magnetic coupling FBG displacement sensor that could only be applied for small scale linear displacement. Hui Yu et al[12] designed a mechanical rotary angle sensor with a sensitivity of 0.743 nm/° and a measuring range of −21°—+21°. A temperature-compensated rotational position sensor was presented by Roberto Montanini[13], achieving a measurement range of ±10° and a sensitivity of 2.43 nm/rad. Chin-Hsing Cheng[14] proposed an optical fiber sensor using an FBG and a piezo-electrical transducer to measure a motor's rotational angle, in which a high sensitivity of 0.459 pm/° was achieved over a measurement range of 0°—270°. The sensors mentioned above cannot detect random rotation angle in the same direction infinitely because there is a limitation for any fiber's ultimate tension. Hao-Jan Sheng, Jin-Hone He et al[15-17] designed a random-rotational FBG-based angle sensor which was composed of two FBGs glued axially on a metal-rod surface, but it cannot detect the rotational velocity of the rotor.

Many other researchers have investigated such sensors using uniform intensity beams or the law of leverage to achieve linear displacement measurement and their temperature correction[18-21], but no room was left for large scale continuous measurement and the conversion of linear displacement to angular measurement. In this paper, we propose a non-contact magnetic coupling and strain measurement method based on a single FBG and circular magnetic railings ruler to acquire the angle information of a rotational objective. By monitoring the red-shift and blue-shift of center wavelength of the FBG, we can simultaneously measure the rotational velocity and the angle displacement.

* This work has been supported by the Program for Cheung Kong Scholars and Innovative Research Team in University (No.IRT1212), the Project Plan of Beijing Municipal Science and Technology Commission (No.Z151100003615010), and the Project Plan of Beijing Municipal Education Commission for Enhancing the Innovation Capability in 2015 (No.TJSHG201510772016).

** E-mail: 15201297184@163.com

The proposed rotational sensor structure is composed of a circular magnetic railings ruler and a magnetic grating ruler sensing probe. As depicted in Fig.1(a), the circular magnetic railings ruler consists of the (N/S polarity) permanent magnet array and a plastic turntable for mounting the permanent magnet array. The structure of magnetic grating ruler sensing probe is shown in Fig.1(b). The plastic enclosure is used for directing the permanent magnet in the vertical direction. The neutral cushioning foam is used to ease the shock generated by the magnetic force. A magnetic head is used for distinguishing N and S polarity, and the FBG is fixed in the core of the magnetic head. Epoxy resin is used to fix the FBG, magnetic head and foam together. The metallic sheath and cone-shaped tube is used to protect the FBG from external disturbances, and fiber optic patch cables and asperity polishing connector (APC) are used to link the light path configuration.

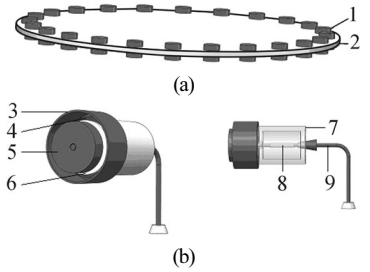

1. circular permanent magnet array; 2. plastic turntable; 3. plastic enclosure; 4. neutral cushioning foam; 5. permanent magnet; 6. epoxy resin; 7. metallic sheath and cone-shaped tube; 8. FBG; 9. fiber optic patch cables and APC

Fig.1 Schematic diagram of system structure consisting of (a) a circular magnetic railings ruler and (b) a magnetic grating ruler sensing probe

Fig.2 shows the structure of the circular magnetic railings ruler, and the magnetic signal on the magnetic ruler with a period of λ is set as a reference ruler. Periodic variations of the magnetic field strength of permanent magnet are in accordance with a sine wave, and the variations of the magnetic force are detected by the magnetic recording head.

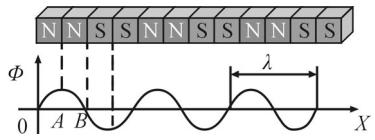

Fig.2 Structure of the circular magnetic railings ruler

The magnetic grating ruler probe with structure shown in Fig.1 is responsible for converting the signal of magnetic force into the signal of angle parameters. A groove with radius of 1 mm is produced by the electric drill at the end of the magnet, and an FBG is connected to the magnetic head whose freedom is limited by a baffle plate construction for only moving in the vertically upward direction. The bottom of the FBG in the strained state is fixed by the epoxy resin which guarantees the intactness of the gratings.

The reflection wavelength λ_B of an FBG is usually expressed as[22]

$$\lambda_B = 2n_{eff}\Lambda, \tag{1}$$

where Λ is the grating period, and Δn_{eff} is the effective refractive index. The most direct affecting factors are the stress and strain parameters which cause the center wavelength of the FBG to shift as

$$\Delta\lambda_B = 2n_{eff}\Delta\Lambda + 2\Delta n_{eff}\Lambda, \tag{2}$$

where Δn_{eff} describes the photo-elastic effect of the optical fiber, and $\Delta\Lambda$ is the elastic deformation of the fiber itself under stress.

Different external stresses are responsible for different variations of Δn_{eff} and $\Delta\Lambda$. In general, since the FBG belongs to an isotropic cylindrical structure, the stress applied on the FBG can be divided into three directions as σ_r, σ_θ and σ_z in a cylindrical coordinate system. Only σ_r and σ_θ exist in the FBG, which are called as transverse stress effect. These three stresses coexist as the body stress as shown in Fig.3.

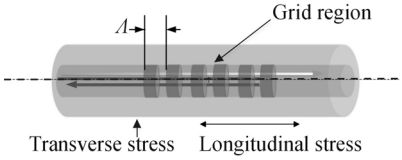

Fig.3 Force-structure analysis of the FBG

As the optical fiber only bears an axial force in the elastic range, Hooke's law can be represented by

$$\begin{cases}\sigma = c\varepsilon \\ F = A\sigma\end{cases}, \tag{3}$$

where σ represents the stress tensor, c represents the modulus of elasticity, ε represents the strain tensor, and A and F represent the cross-sectional area and tensile force of the FBG. Uniform axial stress refers to that stress in the FBG is longitudinally tensile or compressive. When the wavelength shift of the longitudinal strain is related to the strain of the axial FBG, the sensing model is depicted as

$$\frac{\Delta\lambda_B}{\lambda_B} = (1 - p_e)\varepsilon_B, \tag{4}$$

where p_e represents the effective photo-elastic constant, and ε_B represents the axial force of the FBG generated by the strain. The parameter p_e for a germanosilicate fiber at room temperature is 0.216.

The FBG is firmly fixed in the core of the magnetic recording head in the perpendicular direction, and a plastic casing limits the lateral freedom of magnetic head. The magnetic force between magnetic head and the magnetic railings ruler can be written as[23]

$$F_1 = F_0 \sin(\frac{2\pi x}{\lambda}), \tag{5}$$

where F_0 is the maximum amplitude of the magnetic force determined by the distance between the magnetic railings ruler and the probe, λ is the period of the magnetic railings ruler, and

x represents the displacement of the head on the ruler.

By substituting Eqs.(3) and (4) into Eq.(5), combined with the equilibrium of forces during a quasi-static thermodynamic process, the relationship between $\Delta\lambda_B$ and x can be expressed as

$$\Delta\lambda_B=\frac{(1-p_e)\lambda_B}{AC}*\left[F_0\sin(\frac{2\pi x}{\lambda}\pm\frac{\pi}{2}\mu)-mg\right], \tag{6}$$

where m is the mass of the magnetic sensing probe, and g is the gravitational constant.

The relationship between the displacement x and the rotational angle $\Delta\theta$ is expressed as

$$x=\frac{2\pi R\Delta\theta}{360}, \tag{7}$$

where R is the radius of the magnetic ruler. The relationship between $\Delta\lambda_B$ and $\Delta\theta$ can be expressed as

$$\Delta\lambda_B=\upsilon*(F_0\sin\Phi-mg), \tag{8}$$

where $\upsilon=\frac{(1-p_e)\lambda_B}{AC}$, and $\Phi=\frac{4\pi^2R\frac{\Delta\theta}{360}}{\lambda}\pm\frac{\pi}{2}\mu$, $\mu=0$ or 1.

It can be seen that the mass of the magnetic sensing probe has a direct impact on the measurement sensitivity. However, a smaller mass weakens the force between the magnetic ruler and the magnetic head. Thus, it is necessary to choose a proper magnetic sensing probe to improve the accuracy and sensitivity. It can be obtained from Eq.(8) that the change frequency of the FBG center wavelength is inversely proportional to the period of the ruler and is proportional to the radius of the circular magnetic railings ruler. When the circular magnetic railings ruler rotates, according to the formula, we can count the maximum force between the magnetic head and magnetic ruler to obtain the angular velocity of the rotational objective. We use a high-speed interrogator to record the shift of FBG center wavelength of the proposed sensor and the sampling time. Then, we rely on a personal computer (PC) for data processing to obtain the rotational angle, rotational velocity and rotational acceleration of the objective.

In order to validate the feasibility and effectiveness of the proposed non-contact rotational sensor, some comparative experiments are conducted, and the parameters of the sensor are calibrated. The schematic diagram of the experimental setup is shown in Fig.4. We use an electronic speedometer to record the speed of the right end of the DC motor. A magnetic ruler consisting of eight magnetic feet is fixed at the left end of the DC motor, in which a magnetic head is aligned to the grid position. A luminous paper, as a sensitive material to the electronic speedometer, is pasted on the right foot of the DC motor. Broadband light comes from the amplified spontaneous emission (ASE) light source, travels through the optical fiber circulator and the single-mode optical fiber, and is incident on FBG. The reflection parameters of the light (center wavelength of the FBG) are recorded on the Ibsen high-speed interrogator, which interrogates the reflection spectrum. Then, execute a peak search on the PC, and convert the shift of FBG center wavelength to strain.

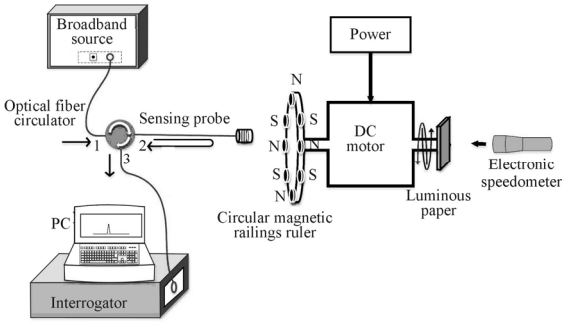

Fig.4 Schematic diagram of the experimental setup

The permanent magnet is made of the second generation of rare-earth permanent magnet, and the geometry is a flat cylinder with diameter of 8 mm and thickness of 2 mm. The circular magnetic railings ruler with eight permanent magnets is located in the circle with diameter of D=110 mm, and the angle between the adjacent permanent magnets with opposite poles is 45°.

A photo of the real magnetic sensing probe is shown in Fig.5(a). The sensor unit uses an epoxy resin named DP420 which is cured for about 24 h at an indoor temperature. The FBG is Gaussian-shape apodized with the grating length of 10 mm. The spectrum of the grating at the initial state measured by a spectrometer AQ6370D with minimum resolution 0.02 nm is shown in Fig.5(b). It can be seen that the center wavelength of the sensing probe after curing is 1 560.278 nm, and the 3 dB bandwidth reaches 0.32 nm. A DC motor is used as the power source, which is a straight biaxial gear motor with a gear ratio of 1:48, an operating voltage of not more than 6 V and a no-load speed of not more than 200 r/min. We adjust the DC voltage to achieve different rotational speeds, and use an electronic speedometer to record the rotational speed and rotational angle of the circular magnetic railings ruler. Set the sampling frequency of the interrogator to 1 000 Hz, and record the center wavelength of the sensing probe with the voltage varying from 0 V to 6 V. The photo of experimental setup is shown in Fig.6.

Reflection spectra of FBG with different rotating angles of 0°, 22.5° and 45° are shown in Fig.7(a), which correspond to the rotating angles of (22.5°+45°×n), (45°+90°×n) and (90°×n), respectively, where n is a positive integer. The relation curve between the rotational angle and the center wavelength of the FBG rotational sensor is shown in Fig.7(b). Fig.7(c) displays the changes of center wavelength of the FBG rotational sensor with different rotational angular velocities, i.e., different voltages. The rotational angular velocity is detected by applying a fast Fourier transformation (FFT) on the change of center wavelength with the same voltage. Simultaneously, the angular velocity is recorded by an intelligent digital speedometer with luminous paper. Then, a linear fitting is done between the angular velocity and a standard value as shown in Fig.7(d).

The N-pole permanent magnets determine the intensity of the force applied on the S-pole magnetic sensing probe. A typical center wavelength for germanosilicate fiber is 1 550 nm at room temperature of 25 °C with a sensitivity of 1.2 pm/με in the theoretical analysis of the strain[24]. We can learn from

Fig.7(a) that the FBG is stretched with a maximum strain up to 445 με with a distance between the sensing probe and circular magnetic ruler of 20 mm.

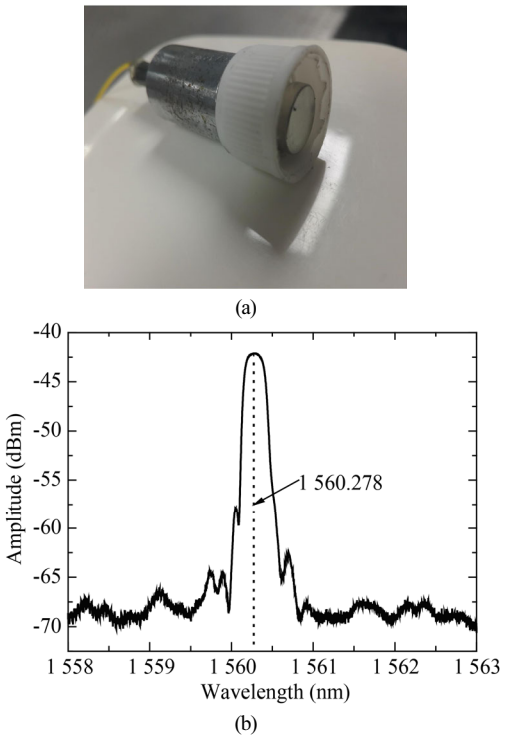

Fig.5 (a) Photo of magnetic sensing probe; (b) Sensor spectrum

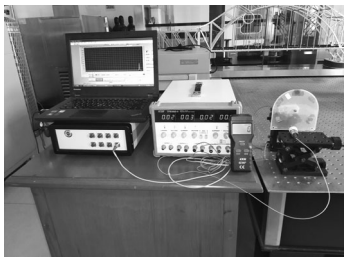

Fig.6 Experimental setup photo

Fig.7(b) represents that the lower peak appears earlier than the higher peak, so the circular magnetic railings ruler rotates counterclockwise. The higher peak represents that the probe faces the N pole, and the center wavelength hardly changes when the probe walks through the area between the N pole and S pole. Due to the baffle plate of the FBG package which limits the freedom, the response cannot be repulsive. However, the presence of bubbles below the S-pole sensing probe makes contribution to the repulsive force, leading to the center wavelength of the valley (1 560.266 nm) smaller than 1 560.278 nm. The modified mathematical model can be considered as the superposition of the sine function. Thus, it is necessary to modify the model of Eq.(8) as

$$\Delta\lambda_B = \upsilon \cdot \left[F_0 \sum (\sin \Phi) - mg \right], \tag{9}$$

and the specific angle transfer mathematical model for this experiment is expressed as

$$\begin{aligned}\Delta\lambda_B = {} & 0.184\,6\cdot\sin(0.999\,8\cdot 4\cdot\alpha - 1.567) + \\ & 0.067\,57\cdot\sin(0.010\,31\cdot 4\cdot\alpha + 1.434) + \\ & 0.045\,79\cdot\sin(2.001\cdot 4\cdot\alpha + 1.553).\end{aligned} \tag{10}$$

We can know from Fig.7(b) that the maximum deviation between the angle transfer mathematical model and the experimental result is only 1.25°, just happening at (67.5°+90°·m), where m is a positive integer. Thus, theoretical analysis and experimental results of rotational angle coincide with each other. From Fig.7(c), we can see the periodic variations

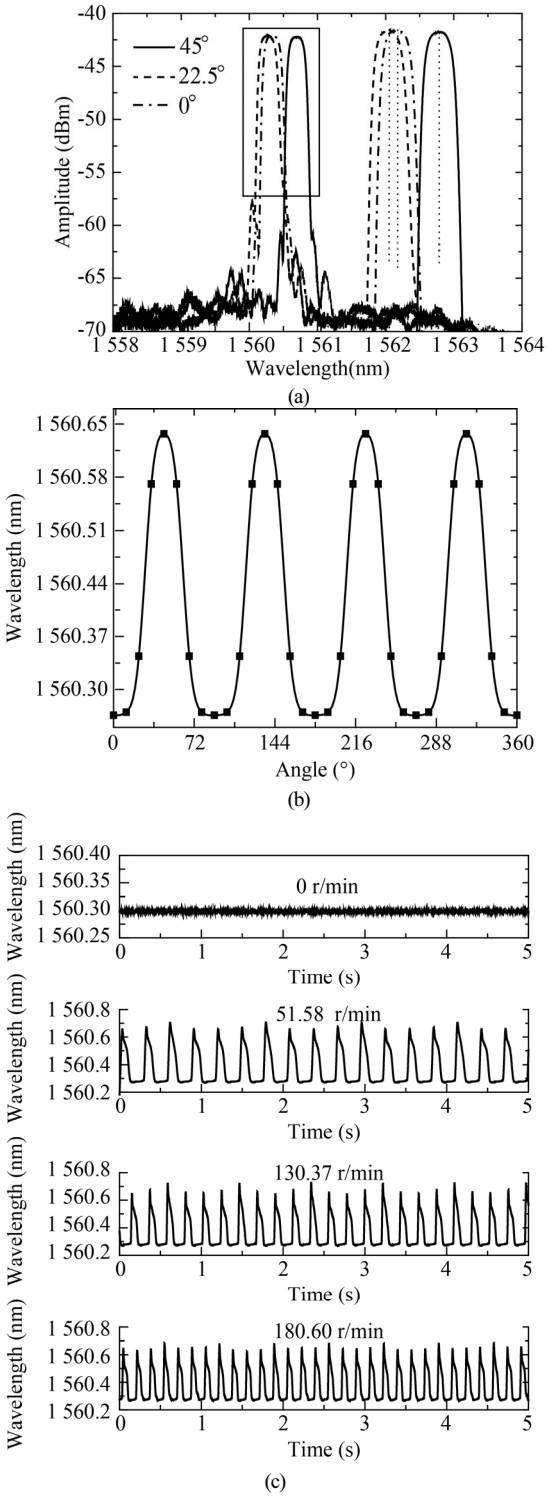

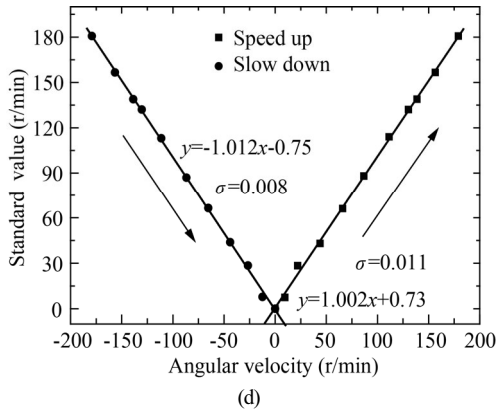

(d)

Fig.7 (a) Reflection spectra of FBG with different rotating angles of 0°, 22.5° and 45°; (b) Relation curve between the rotational angle and center wavelength; (c) The changes of center wavelength with different driving voltages (different rotational angular velocities); (d) Fitting curve between the angular velocity and the standard value

of FBG center wavelength at different driving voltages. Increasing the driving voltage and the rotational angular velocity of the turntable can both lead to a shorter variation period of the center wavelength. The fitting results show a great linearity of up to 0.998 and a standard error of about 0.01 in the range from 0 r/min to 180.6 r/min. The ratio of velocity results measured by the electronic speedometer and the FBG sensing probe is 1.01. We can know that measuring error can be reduced by the miniaturization of sensor. The noise phenomenon appears because the lateral freedom of the permanent magnet in the probe is not completely limited and there are some vibrations generated by the rotation of the motor.

A non-contact rotational sensor based on an FBG combined with a coupled magnetic field is designed and analyzed both theoretically and experimentally. An angle transfer mathematical model is built to study the relationship between the shift of center wavelength of the embedded FBG and the rotational angle. Moreover, a modified model is realized with the proposed experiment on the measurement of rotational angle.

If the sensor is used for quasi-static non-contact rotational measurement, it will require further study for the discrimination of strain and temperature. The dynamic frequency response characteristics of the sensing probe must be optimized when it is used to measure a high-speed rotating objective.

References

[1] W. B. Gan, C. Zhang, D. Y. Tang and F. Liu, Semiconductor Optoelectronics **33**, 795 (2012).

[2] J. Hao, J. H. Ng and S. Takahasi, Fiber Bragg Grating Sensor: US, US7702190, 2010.

[3] Q. P. Liu, J. Y. Hui, X. G. Qiao, Z. A. Jia, H. W. Fu, D. K. Yu and H. Gao, Journal of Optoelectronics·Laser **27**, 468 (2016). (in Chinese)

[4] B. Liu, Y. T. Dai, X. Zhou Xian, M. Zou and Joseph Muna Karanja, Journal of Optoelectronics·Laser **26**, 1860 (2015). (in Chinese)

[5] Z. G. Jia, L. Ren, H. N. Li, M. F. Ren and Q. Z. Huang, Chinese Journal of Lasers **37**, 1298 (2010). (in Chinese)

[6] L. T. Li, D. S. Zhang, X. Y. Wen and S. S. Peng, Chinese Optics Letters **13**, 100601 (2015).

[7] Y. Cao, Y. F. Yang, X. F. Yang and Z. R. Tong, Chinese Optics Letters **10**, 030605 (2012).

[8] Y. P. Zhang, Y. L. Xu and Y. T. Wang, Chinese Journal of Scientific Instrument **35**, 147 (2014). (in Chinese)

[9] X. Y. Li, W. W. Ling, Y. H. Wei and Z. L. Xu, Chinese Optics Letters **13**, 090603 (2015).

[10] S. C. Tao, X. P. Dong and B. W. Lai, Optics Communications **372**, 44 (2016).

[11] J. Wang, B. Liu, F. T. Zhang and D. S. Jiang, Nanotechnology and Precision Engineering **6**, 468 (2008).

[12] H. Yu, X. Yang, Z. Tong, Y. Cao and A. Zhang, IEEE Sensors Journal **11**, 1233 (2011).

[13] R. Montanini and S. Pirrotta, Sensors and Actuators A: Physical **132**, 533 (2006).

[14] C. H. Cheng, S. C. Hung and W. F. Liu, Microwave and Optical Technology Letters **56**, 1449 (2014).

[15] H. J. Sheng, P. T. Tsai, W. Y. Lee, G. R. Lin, H. T. Sun, D. W. Huang and W. F. Liu, IEEE Sensors Journal **12**, 1436 (2012).

[16] H. J. Sheng, G. R. Lin, P. T. Tsai, C. A. Yang, M. H. Kuo, H. T. Sun, M Y. Fu and W. F. Liu, Random-Rotational Angle Sensor Based on Fiber Bragg Gratings, 17th Opto-Electronics and Communications Conference, 192 (2012).

[17] J. H. He, P. T. Tsai, H. J. Sheng, M. S. Lin, H. T. Sun, W. F. Liu, G. R. Lin and M. F. Tsai, A Rotational Angle Sensor Based on Fiber Bragg Gratings, 6th International Conference on Advanced Infocomm Technology, 111 (2014).

[18] C. J. Moreno-Hernández, D. Monzón-Hernández, A. Martínez-Ríos, D. Moreno-Hernández and J. Villatoro, IEEE Photonics Technology Letters **27**, 379 (2015).

[19] D. S. Xu, J. H. Yin, Z. Z. Cao, Y. L. Wang, H. H. Zhu and H. F. Pei, Measurement **46**, 200 (2013).

[20] X. F. Yang, H. Yu, P. Wang, Z. R. Tong , J. T. Zhao and Q. Li, Journal of Optoelectronics·Laser **21**, 1156 (2010). (in Chinese)

[21] L. Z. Cui, Y. Jiang and Y. H. Liu, Acta Photonica Sinica **40**, 1667 (2011). (in Chinese)

[22] Z. H. Gao, X. H. Chen and D. L. Peng, Optics and Precision Engineering **23**, 93 (2015).

[23] Jin Li, Magnetic Grid Displacement Sensor, Mechanical Engineering and Automation **1**, 200 (2014). (in Chinese)

[24] B. Liu, W. C. Niu, Cheng, Y. F. Yang, J. H. Luo, Y. Cao, G. Y. Kai, W. G. Zhang and X. Y. Dong, Chinese Journal of Scientific Instrument **27**, 42 (2006). (in Chinese)